Proxy-based evidence that future climate may be less predictable due to ice melting

Celia Martin-Puertas[1], Armand Hernandez[2], Eulogio Pardo Iguzquiza[3], Laura Boyall[1], Chris Brierley[4], Zhiyi Jiang[4], Rik Tjallingii[5], Simon Blockley[1], Francisco Javier Rodríguez-Tovar[6]

[1] Department of Geography, Royal Holloway University of London, Egham, Surrey, TW20 0EX, UK

[2] Universidade da Coruña, GRICA Group, Centro de Investigacións Científicas Avanzadas (CICA), Faculty of Sciences, A Coruña, Spain

3 Instituto Geológico y Minero de España (IGME), Ríos Rosas 23, 28001 Madrid, Spain

[4] Department of Geography, University College London, London, UK

[5] Climate Dynamics and Landscape Evolution. Helmholtz Zentrum GFZ-Potsdam, Potsdam D-14773, Germany

[6] Departamento de Estratigrafía y Paleontología, Universidad de Granada, Granada, Spain

The oscillatory behaviour of the climate system on decadal timescales beyond the instrumental record is hard to quantify. Yet knowledge of it is vital to support climate predictions and to put current changes in context of past experiences. We investigate the recurrent component of weather and climate variability in the North Atlantic sector during the Holocene in proxy data. We apply time-frequency analysis to both an annually-laminated climate record from a lake in England, and the Atlantic Meridional Overturning Circulation in a long transient simulation to demonstrate that decadal variability was consistent over the last 6,700 years and prior to 8,500 years before present, which was predominantly linked to solar and ocean forcing. Between these dates, climate variability was dampened on decadal timescales. Our results suggest that meltwater discharge into the North Atlantic and the subsequent hydrographic changes, from the opening of the Hudson Bay until the final collapse of the Laurentide Ice sheet, disrupted the regular climate patterns: suspending the decadal cyclic signals, and lowering the predictable signal of the climate system. Our results have relevance for near-term climate predictions given the current acceleration of the Greenland Ice Sheet melting in response to global warming.

According to the most recent assessment of the Intergovernmental Panel on Climate Change, tipping points of the Earth's climate system – such as the melting of the Greenland Ice Sheet (GrIS) – could happen from 1.5 °C of warming[1] with direct impact on the Atlantic Meridional Overturning Circulation (AMOC) and, consequently, European climate[2]. Near-term (annual to decadal) climate predictions play a key role in anticipating climate change and reducing the reaction time to any potential alert[3]. Sources of decadal predictability includes radiative forcing[4] and internal variability associated mainly with the sea surface temperature, ocean heat content and atmospheric teleconnections[3]. The reliability of decadal predictions depends on how well the models capture the predictable signal contained within the external drivers and initial conditions[3]. And these are tested by performing retrospective climate model forecasts (or 'hindcasts'), which are then compared with observations[5,6]. Despite decadal predictions systems demonstrating skilful surface temperature forecasts[6] and increasingly accurate predictions of precipitation and atmospheric circulation patterns[5,7,8], there are concerns about whether interdecadal and multidecadal climate cycles could be modulated by the cumulative response to high-frequency radiative forcing since the pre-industrial period[9]. Observations are insufficient to test these concerns as they only cover a few decadal cycles[10], and the climate community has urgently called for long climate-proxy records with sufficient precision and accuracy to test for decadal predictable signals in weather and climate variability over longer time intervals[7, 9,11,12].

The present interglacial period, the Holocene, is an ideal interval to investigate decadal climate variability because it covers several millennia with changing orbital configurations[13]. Proxy-based and model-tested climate reconstructions show evidence for multidecadal recurrent patterns during the Late Holocene resembling present modes of climate variability such as the El Niño Southern Oscillation, the Pacific decadal variability, the Atlantic Multidecadal Variability (AMV) and the North Atlantic Oscillation (NAO); but reconstructions are scarce and/or inconsistent for the rest of the Holocene[11,14]. Major issues include the non-stationarity of the climate-proxy relationship, and the lack of very high temporal precision in many reconstructions of past climate variability, from continuous, long-term proxy records[11].

To investigate Holocene decadal climate variability in the North Atlantic (NA) sector, we use the annually-laminated (varved) record of Diss Mere, a lake in central-east England[15] (Fig. 1). We use this location because the British Isles are very sensitive to NA climate (Supplementary Information) and central England temperature is highly correlated with Global Mean Surface Temperature[16,17]. Diss Mere is the only record in the UK that provides continuous, well-dated palaeoclimate proxy data over most of the Holocene[15]. Considering that lower decadal variability leads to less statistical predictability[18], this study aims to test the low-frequency (decadal) recurrent component of the natural Earth's climate system over the past ten millennia and to discuss the role of changing climate states for decadal predictability.

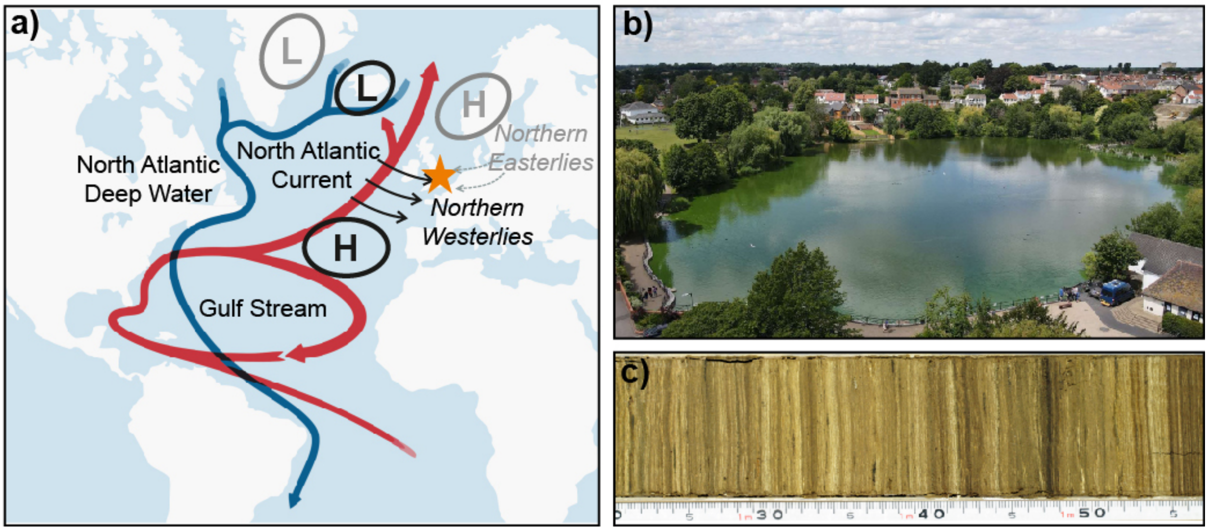

Figure 1. Diss Mere proxy record and regional climatic settings. a) Diss Mere location (yellow star), regional ocean circulation associated with the Atlantic Meridional Overturning Circulation (AMOC) and main sea level air pressure centres in the North Atlantic region today (Supplementary Section 1). Red arrow indicates warm and salty waters and blue arrows indicates cold and fresh waters. Black arrows represent westerlies associated with the main mode of atmospheric circulation, the North Atlantic Oscillation (NAO), and dashed grey arrows show northern easterlies associated with the Scandinavian blocking; b) aerial photo of Diss Mere; c) core photo of a 37 cm section of the laminated sediments of Diss Mere. Depth scale indicates core section depth.

The palaeoclimate proxy record of Diss Mere

Diss Mere (52° 22'N, 1° 6'E; 29 m above sea level) has a sedimentary record for the last 10,500 years[15] (Supplementary Fig. 1). Human activities clearly influence the lake today (Fig. 1b), but did not have a significant impact on the landscape in the catchment area until the Iron Age (roughly 2000 years ago) when annual layers (varves, Fig. 1c) stopped being preserved[19] (Supplementary Fig. 1). Varves are well-preserved from

2.1 to 10.3 thousand years before present (cal. ka BP) and the record is linked to a very robust chronology with a maximum absolute uncertainty of ± 55 years at the beginning of the Holocene[15], but more typically in the range ± 20-30 years (Supplementary Section 2; Supplementary Fig. 1). Annual sedimentation is mainly controlled by limnological processes in response to the annual thermal stratification and mixing cycle of the water column (Supplementary Fig. 2; Supplementary Fig. 3). Catchment processes such as runoff have a minimal impact on the lake. Varves consist of a temperature-induced authigenic calcite layer that precipitates during the summer; and a detritus lamina made of mainly aquatic organic matter filaments and planktonic centric diatom blooms deposited in winter. Lake productivity responds to additional nutrient input from the lake bottom to the photic zone during the winter lake turnover and favoured by wind speed (Supplementary Section 2; Supplementary Table 1).

The summer (temperature sensitive) and winter (wind speed / storminess sensitive) layers evolve independently during the Holocene (Fig. 2a), hence the season and climate driver that control the total varve thickness was changing over time (Fig. 2a). In other words, although this prevents us from linking the total varve thickness to a specific climatic variable through the entire Holocene (e.g. air temperature), variations in varve thickness reflect the annual lake response to climate conditions dominated by one or other of the two seasons, depending on the time window we look at (Fig. 2; Supplementary Fig. 4; Supplementary Fig. 5). Despite the seasonal biases, the varve thickness record provides information about climate conditions at an annual resolution and is, therefore, ideal for investigating decadal variability in this location.

The AMOC plays an important role in the NA and British Isles climate. This is explained by heat transport and an atmosphere-ocean coupling over the Southern Greenland area with impact on modes of variability such as the AMV and NAO[20,21] and their non-stationary interactions operating in this region[22] (Fig. 1a; Supplementary Section 1). To provide evidence supporting the regional climate signal recorded in the Diss Mere varve thickness record, an AMOC time series was extracted from a long transient climate model simulation[23] performed with the CCSM3 climate model (Fig. 2b) and compared with our proxy record. This simulation is forced by changes in orbital configuration, greenhouse gas concentrations, land-sea mask, ice sheet topography and meltwater fluxes[24]. The Diss Mere varve thickness record is well correlated with the strength of the AMOC at Diss Mere's latitude ($r = 0.54$, $p < 0.01$; Fig. 2 a, b). Both the AMOC and the Diss Mere varve thickness record show a multi-millennial gradual increasing trend over the Holocene, following the Holocene global sea surface temperature evolution[25] (Fig. 2c). In addition, the summer component of the total varve thickness, represented by temperature-induced calcite precipitation, is well correlated with the Temperature 12K reconstruction at 30-60°N[26], which includes both marine and terrestrial records.

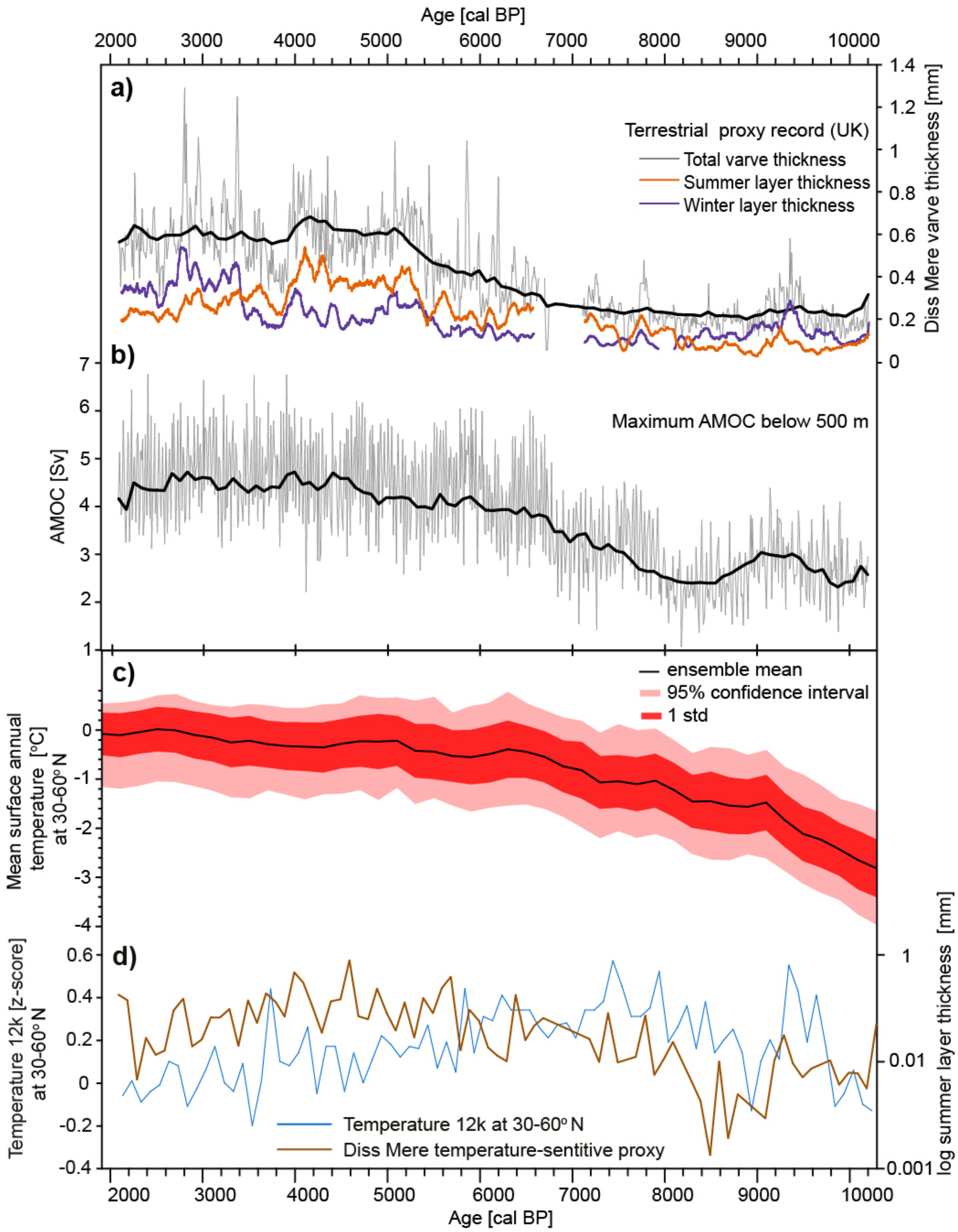
Age [cal BP]
a)
Terrestrial proxy record (UK)
Total varve thickness
Summer layer thickness
Winter layer thickness
Diss Mere varve thickness [mm]
b)
Maximum AMOC below 500 m
AMOC [Sv]
c)
ensemble mean
95% confidence interval
1 std
Mean surface annual temperature [°C] at 30-60° N
d)
Temperature 12k [z-score] at 30-60° N
Temperature 12k at 30-60° N
Diss Mere temperature-sentitive proxy
log summer layer thickness [mm]
Age [cal BP]

Figure 2. Comparison between the terrestrial palaeoclimate proxy record in the UK, AMOC and Holocene temperature reconstructions over the Holocene (10.3 – 2.1 cal. ka BP). a) Varve thickness record from the Lake Diss Mere, UK (52ºN), 10-year averaged in grey, and 100-year averaged in black. 30-yr average summer (winter) in orange (purple); b) timeseries of the maximum AMOC at 52ºN below 500 m (TraCE-21ka simulation. Maximum resolution available is 10-year averaged, in grey. 100-year averaged in black. Data available at: https://www.earthsystemgrid.org/project/trace.html); c) mean surface annual temperature at 30-60ºN based on marine proxy records[25]. d) Comparison between the thickness of the calcite layer in Diss Mere (log scale) and the Temperature 12k[26] at 30-60ºN, which is based on both marine and terrestrial proxy records.

Holocene decadal climate variability and major drivers

High predictability can be assumed with either the predominant low-frequency (decadal timescales) contribution, the presence of spectral peaks, or both[18]. To evaluate the predictable component of the Holocene climate, we applied time-frequency analysis to the Diss Mere total varve thickness and the thickness of the seasonal layers (Methods; Fig. 3a; Supplementary Fig. 4; Supplementary Fig. 5). The Diss Mere spectrograms show significant periodicities on decadal to multidecadal timescales, which can readily be ascribed to: i) quasi-periodicities of solar activity, 11 (up to 14) years Sunspot cycle and 22 years Hale cycle[27]; and ii) the AMV, a 40-88 years oscillatory signals centred in the NA and associated with the AMOC and ocean-atmosphere processes[28] (Fig. 3; Supplementary Fig. 6). These periodicities are recorded in both the varve and the seasonal layers (Supplementary Fig. 4), supporting that the varve thickness record contain information of annual climate variability.

The oscillatory signals were not consistent during the entire Holocene (Fig. 3a). Prior to 9 cal. ka BP, multidecadal to decadal variability responded to cycles of 75 and 22 years only, suggesting that climate behaved in a recurrent way driven by both solar activity[27] and internal variability of the ocean-atmosphere system[29,30]. Critically, however, during the period between 6.8 and 9 cal. ka BP the cyclic signals are much weaker, even absent, which indicates more irregular climate dynamics. From 6.8 cal. ka BP to present, decadal-scale variability is again driven by solar activity and internal ocean-atmosphere forcing, but over a wider range of periodicities than in the early Holocene (Fig. 3a) suggesting a more complex climate system. This could be explained by the development of high-pressure systems over the circum-Baltic regions and eastern Europe as a consequence of the land-sea-ice redistribution associated with changes in the Scandinavian Ice Sheet and the Baltic Sea[31]. Local high-pressure centres should have resulted in new regional atmospheric patterns and teleconnections, likely with a more meridional component, like the present configuration of the sea level pressure centres over the NA and Europe (Fig. 1a).

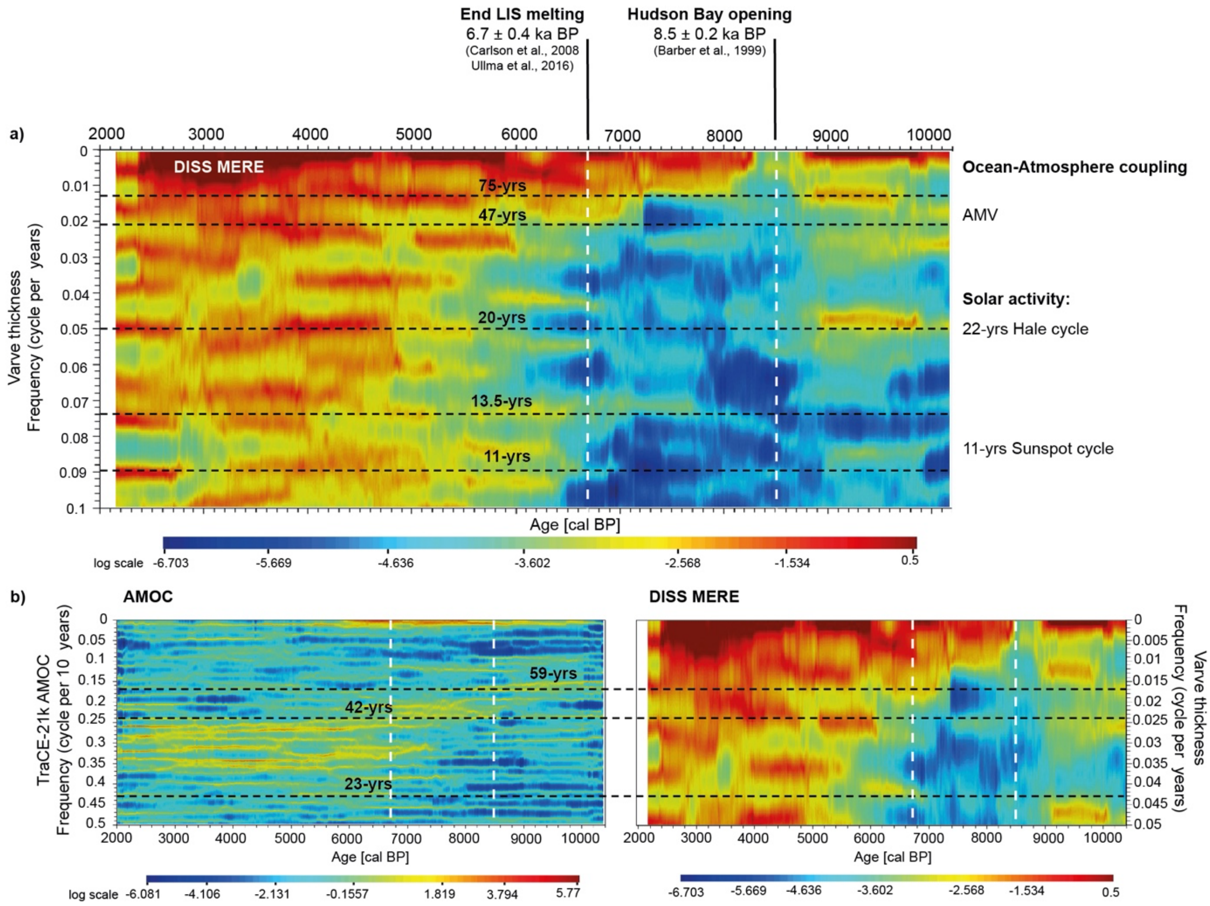

Figure 3. Holocene decadal oscillatory signals in the North Atlantic. a) Maximum entropy spectrogram of the Diss Mere annual varve thickness record. Solar activity and AMV have been identified as major drivers of recurrent decadal and multi-decadal variability (significant level >98%); b) comparison of the AMOC at 52ºN (left) and Diss Mere (right) multi-decadal variability as shown in the maximum entropy spectrograms. The highest output resolution available for the TraCE-21k AMOC simulation is decadal and frequencies higher than 0.05 cycle per year (< 20-year cycles) might not detected. The colour bar (power) is represented in a logarithmic scale. White dashed lines indicate the period of muted decadal to multidecadal variability in the NA region.

Centennial-scale variations are consistent during the entire Holocene, except for a 500-yr episode at 8.3-8.7 cal. ka BP (Fig. 3a). This episode coincides with the opening of the Hudson Bay at 8.5 $\pm$ 0.2 cal. ka BP and a significant increase in freshwater input into the NA that could trigger the so-called 8.2 ka event[32,33]. The opening of the Hudson Bay, the drainage of Lake Agassiz[32] and the collapse of the Laurentide ice saddle[34] led to major changes in orography, reorganisation of the hydrography along the NE America margin freshwater pulses to different part of the NA[35–37], and changes in sea level and regional albedo[38]. This resulted in climate instability with impact on the AMOC[39–41] and regional atmospheric circulation[42] for a few millennia. The final Laurentide Ice Sheet deglaciation is dated at 6.7 $\pm$ 0.4 cal. ka BP[35,43], coinciding with the activation of the Labrador Sea Water formation that define the current configuration of the NA circulation[44] and the onset of consistent decadal climate variability as shown in this study (Fig. 3a). This scenario connects a cascade of changes in ice dynamics, ocean circulation and atmospheric responses that led to a new climate state which, according to our results, had potentially predictive skills on decadal timescales.

The simulated AMOC at 52°N (Fig. 2b) is a scaled version of a maximum strength at lower latitudes, increasing from its minimum associated with a rapid meltwater pulse imposed at ca. 8.5 cal. ka BP. From ca. 6.8 cal. ka BP, the AMOC stabilises once the meltwater flux from the Hudson Strait ceases[24]. Like the proxy record, time-frequency analysis of the AMOC simulation (Fig. 3b, Supplementary Fig. 6) shows a marked increase in power at interdecadal timescales from 7.4-6.8 cal. ka BP to present. The oscillatory signal is much weaker prior to that date suggesting that freshwater fluxes had an impact on both strengthen and decadal variability of the AMOC. The potential link between muted decadal-scale climate variability and sea ice has been already discussed in the last two millennia[14,45] and the last glacial period[46]; and here we add the role of the Laurentide ice sheet melting into the discussion.

Considerations for decadal prediction research

We present a long-term re-evaluation of evidence for low-frequency climate oscillations during the Holocene in proxy data, which confirms that decadal climate variability was actively present during the last seven millennia, providing persistent predictability to the coupled climate system. However, our study also shows that this predictable component was vulnerable to changes in continental ice-sheets. Our findings suggest that the freshwater fluxes following the opening of the Hudson Bay and the associated hydrographic changes at 8.5 ± 0.2 cal. ka BP had a disruptive effect on the Earth's climate system. This led to suppressed decadal-scale variability mediated via impacts on ocean circulation and associated air-sea feedbacks, with implications for climate predictability in the subsequent two thousand years. Once the Northern Hemisphere ice cap was stable again at 6.7 ± 0.4 cal. ka BP, the Earth's climate system reached a new equilibrium state with a marked increase in both the amplitude of response (Fig. 2) and its variability on decadal to multidecadal scales (Fig. 3).

A parallelism can be established between the palaeo-evidence presented in this study around 8.5 cal. ka BP and the near-term future, in which the current and accelerating melt of the ice-sheets may result in a less predictable climate system. However, there is still a large uncertainty concerning the possible linkages between Greenland melt and AMOC[1,47], partly due to the spatiotemporal complexity of the NA ocean and its stability[47,48]. The estimated GrIS melting rate under a high emission scenario is equivalent to the freshwater fluxes that triggered the 8.2 ka event[49]. However, compared to the early Holocene event, the ongoing and future Greenland meltwaters flow into the coastal areas of Greenland instead of directly into the Labrador Sea[44], which might have a different impact on the AMOC and North Atlantic predictability. Despite its potentially critical impacts on the climate system, Greenland melt has been widely neglected in future climate projections and has never been considered in decadal climate prediction. While challenging due to the relatively poor understanding of the processes, the lack of adequate long-term observations and the technical difficulties to simulate their effect, our findings urge considering the impact of GrIS meltwater fluxes on decadal prediction system, as well as warning of less predictability when temperatures, but not sea level, have stabilised.

References

1. Special Report on the Ocean and Cryosphere in a Changing Climate —. https://www.ipcc.ch/srocc/.
2. Moffa-Sánchez, P. & Hall, I. R. North Atlantic variability and its links to European climate over the last 3000 years. *Nat. Commun.* **8**, 1726 (2017).
3. Kushnir, Y. *et al.* Towards operational predictions of the near-term climate. *Nat. Clim. Change* **9**, 94–101 (2019).
4. Meehl, G. A. *et al.* Decadal Prediction: Can It Be Skillful? *Bull. Am. Meteorol. Soc.* **90**, 1467–1486 (2009).
5. Smith, D. M. *et al.* North Atlantic climate far more predictable than models imply. *Nature* **583**, 796–800 (2020).
6. Boer, G. J. *et al.* The Decadal Climate Prediction Project (DCPP) contribution to CMIP6. *Geosci. Model Dev.* **9**, 3751–3777 (2016).

7. Smith, D. M. *et al.* Robust skill of decadal climate predictions. *Npj Clim. Atmospheric Sci.* **2**, 13 (2019).
8. Dunstone, N. *et al.* Skilful interannual climate prediction from two large initialised model ensembles. *Environ. Res. Lett.* **15**, 094083 (2020).
9. Mann, M. E., Steinman, B. A. & Miller, S. K. Absence of internal multidecadal and interdecadal oscillations in climate model simulations. *Nat. Commun.* **11**, 49 (2020).
10. O'Reilly, C. H., Woollings, T. & Zanna, L. The Dynamical Influence of the Atlantic Multidecadal Oscillation on Continental Climate. *J. Clim.* **30**, 7213–7230 (2017).
11. Hernández, A. *et al.* Modes of climate variability: Synthesis and review of proxy-based reconstructions through the Holocene. *Earth-Sci. Rev.* **209**, 103286 (2020).
12. Rehfeld, K., Hébert, R., Lora, J. M., Lofverstrom, M. & Brierley, C. M. Variability of surface climate in simulations of past and future. *Earth Syst. Dyn.* **11**, 447–468 (2020).
13. Wanner, H. *et al.* Mid- to Late Holocene climate change: an overview. *Quat. Sci. Rev.* **27**, 1791–1828 (2008).
14. Lapointe, F. *et al.* Annually resolved Atlantic sea surface temperature variability over the past 2,900 y. *Proc. Natl. Acad. Sci.* **117**, 27171–27178 (2020).
15. Martin-Puertas, C. *et al.* The first Holocene varve chronology for the UK: Based on the integration of varve counting, radiocarbon dating and tephrostratigraphy from Diss Mere (UK). *Quat. Geochronol.* **61**, 101134 (2021).
16. Sutton, R., Suckling, E. & Hawkins, E. What does global mean temperature tell us about local climate? *Philos. Trans. R. Soc. Math. Phys. Eng. Sci.* **373**, 20140426 (2015).

17. Hawkins, E. *et al.* Estimating Changes in Global Temperature since the Preindustrial Period. *Bull. Am. Meteorol. Soc.* **98**, 1841–1856 (2017).
18. Privalsky, V. E. Statistical predictability and spectra of air temperature over the northern hemisphere. *Tellus A* **35A**, 51–59 (1983).
19. Peglar, S. M. The mid-Holocene Ulmus decline at Diss Mere, Norfolk, UK: a year-by-year pollen stratigraphy from annual laminations. *The Holocene* **3**, 1–13 (1993).
20. Rodwell, M. J., Rowell, D. P. & Folland, C. K. Oceanic forcing of the wintertime North Atlantic Oscillation and European climate. *Nature* **398**, 320–323 (1999).
21. Sutton, R. T. & Hodson, D. L. R. Atlantic Ocean Forcing of North American and European Summer Climate. *Science* **309**, 115–118 (2005).
22. Comas-Bru, L. & Hernández, A. Reconciling North Atlantic climate modes: revised monthly indices for the East Atlantic and the Scandinavian patterns beyond the 20th century. 16 (2018).
23. Transient Simulation of Last Deglaciation with a New Mechanism for Bølling-Allerød Warming. https://www.science.org/doi/10.1126/science.1171041 doi:10.1126/science.1171041.
24. He, F. Simulating Transient Climate Evolution of the Last deglaciation with CCSM3. 161.
25. Osman, M. B. *et al.* Globally resolved surface temperatures since the Last Glacial Maximum. *Nature* **599**, 239–244 (2021).
26. Kaufman, D. *et al.* A global database of Holocene paleotemperature records. *Sci. Data* **7**, 115 (2020).
27. Hale, G. E., Ellerman, F., Nicholson, S. B. & Joy, A. H. The Magnetic Polarity of Sun-Spots. *Astrophys. J.* **49**, 153 (1919).

28. Schlesinger, M. E. & Ramankutty, N. An oscillation in the global climate system of period 65–70 years. *Nature* **367**, 723–726 (1994).

29. Delworth, T. L. & Mann, M. E. Observed and simulated multidecadal variability in the Northern Hemisphere. *Clim. Dyn.* **16**, 661–676 (2000).

30. Kerr, R. A. A North Atlantic Climate Pacemaker for the Centuries. *Science* (2000) doi:10.1126/science.288.5473.1984.

31. Yu, G. & Harrison, S. P. Holocene changes in atmospheric circulation patterns as shown by lake status changes in northern Europe. *Boreas* **24**, 260–268 (1995).

32. Barber, D. C. *et al.* Forcing of the cold event of 8,200 years ago by catastrophic drainage of Laurentide lakes. *Nature* **400**, 344–348 (1999).

33. Gregoire, L. J., Ivanovic, R. F., Maycock, A. C., Valdes, P. J. & Stevenson, S. Holocene lowering of the Laurentide ice sheet affects North Atlantic gyre circulation and climate. *Clim. Dyn.* **51**, 3797–3813 (2018).

34. Matero, I. S. O., Gregoire, L. J., Ivanovic, R. F., Tindall, J. C. & Haywood, A. M. The 8.2 ka cooling event caused by Laurentide ice saddle collapse. *Earth Planet. Sci. Lett.* **473**, 205–214 (2017).

35. Carlson, A. E. *et al.* Rapid early Holocene deglaciation of the Laurentide ice sheet. *Nat. Geosci.* **1**, 620–624 (2008).

36. Hillaire-Marcel, C., de Vernal, A. & Piper, D. J. W. Lake Agassiz Final drainage event in the northwest North Atlantic. *Geophys. Res. Lett.* **34**, (2007).

37. Carlson, A. E., Clark, P. U., Haley, B. A. & Klinkhammer, G. P. Routing of western Canadian Plains runoff during the 8.2 ka cold event. *Geophys. Res. Lett.* **36**, (2009).

38. Gregoire, L. J., Payne, A. J. & Valdes, P. J. Deglacial rapid sea level rises caused by ice-sheet saddle collapses. *Nature* **487**, 219–222 (2012).

39. Clark, P. U. *et al.* Freshwater Forcing of Abrupt Climate Change During the Last Glaciation. *Science* **293**, 283–287 (2001).
40. Thornalley, D. J. R. *et al.* Long-term variations in Iceland–Scotland overflow strength during the Holocene. *Clim. Past* **9**, 2073–2084 (2013).
41. Ayache, M., Swingedouw, D., Mary, Y., Eynaud, F. & Colin, C. Multi-centennial variability of the AMOC over the Holocene: A new reconstruction based on multiple proxy-derived SST records. *Glob. Planet. Change* **170**, 172–189 (2018).
42. Wassenburg, J. A. *et al.* Reorganization of the North Atlantic Oscillation during early Holocene deglaciation. *Nat. Geosci.* **9**, 602–605 (2016).
43. Ullman, D. J. *et al.* Final Laurentide ice-sheet deglaciation and Holocene climate-sea level change. *Quat. Sci. Rev.* **152**, 49–59 (2016).
44. Hillaire-Marcel, C., de Vernal, A., Bilodeau, G. & Weaver, A. J. Absence of deep-water formation in the Labrador Sea during the last interglacial period. *Nature* **410**, 1073–1077 (2001).
45. Lapointe, F. & Bradley, R. S. Little Ice Age abruptly triggered by intrusion of Atlantic waters into the Nordic Seas. https://www.science.org/doi/10.1126/sciadv.abi8230 doi:10.1126/sciadv.abi8230.
46. Sirocko, F. *et al.* Muted multidecadal climate variability in central Europe during cold stadial periods. *Nat. Geosci.* **14**, 651–658 (2021).
47. Swingedouw, D. *et al.* AMOC Recent and Future Trends: A Crucial Role for Oceanic Resolution and Greenland Melting? *Front. Clim.* **4**, (2022).
48. Moffa-Sánchez, P. *et al.* Variability in the Northern North Atlantic and Arctic Oceans Across the Last Two Millennia: A Review. *Paleoceanogr. Paleoclimatology* **34**, 1399–1436 (2019).

49. Aguiar, W. *et al.* Magnitude of the 8.2 ka event freshwater forcing based on stable isotope modelling and comparison to future Greenland melting. *Sci. Rep.* **11**, 5473 (2021).

50. Aschwanden, A. *et al.* Contribution of the Greenland Ice Sheet to sea level over the next millennium. *Sci. Adv.* **5**, eaav9396 (2019).

Corresponding author: celia.martinpuertas@rhul.ac.uk

Acknowledgements

This study was funded by the Royal Society. CM-P was supported by a Royal Society Dorothy Hodgkin Fellowship (ref: DH150185) and a UKRI Future Leaders Fellowship (MR/W009641/1). AH is supported by the Spanish Ministry of Science and Innovation through the Ramón y Cajal Scheme [RYC2020-029253-I]. We thank Pablo Ortega and Eduardo Moreno-Chamarro for valuable discussions. We also thank Amy Walsh and George Biddulph for varve counting; Iñaki Valcarcel, Poppy Harding and Joshua Pike between others for their contribution to the lake monitoring survey; Anni Zhao for plotting complementary climate datasets that helped with the interpretation of the proxy record; Prof. Achim Brauer and his team for lake coring.

Author contribution

C.M-P. led the research, performed the palaeolimnological study and wrote the paper. A.H. contributed significantly to the discussion and interpretation of the results and the writing of the manuscript. E.P.I performed the maximum entropy analysis of the proxy data and AMOC simulation and contributed to the writing of the manuscript. LB contributed to the palaeoclimate interpretation of the proxy record and the writing of the manuscript. C.B and Z.J. analysed the AMOC in TraCE-21ka simulation, interpreted the results related to the AMOC simulation, and contributed to the writing of the manuscript. S.B. contributed to the chronology of the proxy record. F.J.R.T visualized the potential of the proxy record for cyclostratigraphy. All co-authors contributed to the discussion of the results and provided feedback on the manuscript.

Methods

Proxy-based methods

Four parallel sediment cores were obtained in September 2016 from the deepest part of Diss Mere, using a 90 mm diameter UWITEC piston corer (DISS16-A, B, C and D). Additionally, two gravity cores of 1m length (DISS16-1S and 2S) were collected from the same area to record the present sediments at the sediment-water interface. The maximum distance between cores is 5 m. Core DISS16- A (15.2 m of length) is composed of eight continuous core sections of ca 2 m length and core DISS16-B (13.28 m of length) is made of seven continuous core sections of ca 2 m. Core A was recovered from the water/sediment interface whereas core B starts 100 cm below core A to create an overlap. Cores DISS16-C (7.72 m of length, 4 cores sections of 2 m long) and DISS16-D (5.81 m of length, 3 core sections of 2 m long) start at 6 m and 7 m of sediment depth, respectively (Supplementary Figure 1). These cores provide two additional parallel sequences of the varved sediment. The cores were correlated using a total of 67 macroscopic visible and 129 microscopic marker layers and the best-preserved sections were combined to construct the continuous composite profile DISS-16 of 14.5 m length.

Samples for petrographic thin sections were taken from the four piston cores along the finely-laminated sequence (8.88–13.15 m of sediment depth). Fresh sediment blocks

(10 × 2 × 1 cm) were extracted from the open, split core surface with 2 cm overlaps to enable continuous microfacies analysis, including correlation of marker layers. Thin sections were prepared according to a standard procedure including freeze-drying and impregnation with epoxy resin. Detailed microfacies analysis, varve counting, and varve and sub-varve layer thickness measurements were performed on the petrographic thin sections using a Leica (M205C) stereo-zoom petrological microscope with plane- and cross-polarised light, at 80x. Varve counting and varve thickness measurements were performed for each seasonal layer along the ca 4.2 m long sequence of varved sediments[15].

Micro-XRF scanning maps (Supplementary Fig.2) were measured on impregnated sediment blocks used for thin-section preparation. Elemental mapping analyses were performed in a vacuum chamber at 50 μm resolution with a M4 Tornado micro-XRF scanner. This micro-XRF scanner is equipped with a Rh X-ray source (50 kV, 0.60 mA) in combination with polycapillary X-ray optics, to produce a high intensity irradiation spot of about 20 μm that allows fast measurement times (30 ms).

Water temperature was measured in situ using two nKe thermistors attached to sediment traps at 1 m (epilimnion) and 5.5 m (hypolimnion) of water depth from June 2018 to June 2021. Data were recorded every 10 minutes and daily averages were calculated. The meteorological data was obtained from the Tibenham Airfield meteorological station (13 km from Diss Mere from 2018-2021).

Simulated AMOC

The "TraCE-21ka" simulation[23] uses the palaeoclimate version[51] of CCSM3, with a low-resolution atmosphere (T31) and ocean (gx3v5, roughly 3°). It is coupled with a sea ice model and a land surface model that incorporates dynamic vegetation. Greenhouse gas concentration follow ice-core measurements with constant aerosol concentrations[24]. The ICE-5G reconstruction[52] is used to define the evolution of the land-sea mask, ice sheet topography and meltwater fluxes. The AMOC shown is the maximum meridional overturning stream function below 500 m at the latitude of Diss Meer (52°N), which is roughly one third of the strength at 30°N. Single-forcing experiments demonstrate the importance of the imposed meltwater fluxes in defining the magnitude and timing of changes in the AMOC[24].

Statistical analyses

The correlation between the varve thickness record and the simulated AMOC was computed on a common temporal resolution (10 years) and resulting in a coefficient of 0.54. The role of autocorrelation in determining the effective sample size, and hence the statistical significance, was assessed using an isospectral null model via the PyleoClim python package[53]. The corelation remains statistically significant, but note this arises from the long-term trends over the Holocene.

Maximum entropy spectral analysis (MESA) is a high-resolution spectral estimator that has been widely used in geosciences[54]. It is based on choosing the spectrum that corresponds to the most random (i.e., unpredictable) time series whose covariance function coincides with the known values. The solution to choosing the maximum entropy spectrum is equal to the autoregressive estimator of the power spectrum[55]. MESA is especially suitable for estimating the power spectrum of short time series and thus it is well suited for estimating the spectrogram[56]. The power spectrum and the spectrogram of the varves time series were estimated by using MESA. The power spectra significance test has been done with a defined confidence level of 95% with most of the peaks higher than 98%.

Wavelet power spectrum plots were computed using the 'PyCWT' package in Python. The mother wavelet was taken to be a Morlet wavelet with ω_0 of 6. The power spectra significance test has also been done with a defined significance level of 95% (The power is significant where the ratio *power / sig95 > 1*)[57].

Data availability

The varve thickness data that support the findings of this study are available on PANGAEA https://doi.pangaea.de/10.1594/PANGAEA.944411. Timeseries data of the maximum AMOC at 52oN below 500 m (TraCE-21ka simulation) are available at: https://www.earthsystemgrid.org/project/trace.html).

References

51. Yeager, S. G., Shields, C. A., Large, W. G. & Hack, J. J. The Low-Resolution CCSM3. J. Clim. 19, 2545–2566 (2006).

52. Peltier, W. R. GLOBAL GLACIAL ISOSTASY AND THE SURFACE OF THE ICE-AGE EARTH: The ICE-5G (VM2) Model and GRACE. Annu. Rev. Earth Planet. Sci. 32, 111–149 (2004).

53. Khider, D., Emile-Geay, J., Zhu, F., James, A., Landers, J., Ratnakar, V. & Gil, Y. Pyleoclim: Paleoclimate Timeseries Analysis and Visualization with Python. Preprint at https://doi.org/10.1002/essoar.10511883.1

54. Pardo-Igúzquiza, E. & Rodríguez-Tovar, F. J. MAXENPER: a program for maximum entropy spectral estimation with assessment of statistical significance by the permutation test. Comput. Geosci. 31, 555–567 (2005).

55. Ulrych, T. J. & Bishop, T. N. Maximum entropy spectral analysis and autoregressive decomposition. Rev. Geophys. 13, 183–200 (1975).

56. Pardo-Igúzquiza, E. & Rodríguez-Tovar, F. J. Maximum entropy spectral analysis of climatic time series revisited: Assessing the statistical significance of estimated spectral peaks. J. Geophys. Res. Atmospheres 111, (2006).

57. Liu, Y., Liang, X. S. & Weisberg, R. H. Rectification of the Bias in the Wavelet Power Spectrum. J. Atmospheric Ocean. Technol. 24, 2093–2102 (2007).